

Numerical Investigation of Turbulent Mass Transfer in a 90° Bend

Asadi, Tahereh; Nasr Esfahany, Mohsen*⁺

Department of Chemical Engineering, Isfahan University of Technology, Isfahan, I.R. IRAN

ABSTRACT: This paper presents a numerical study of local mass transfer coefficients in a 90° bend using the RNG version of $k-\varepsilon$ model to include the influence of curvature on the turbulent transport. Simulations were performed for flow through a 90°, 3-D bend for Reynolds numbers of 13500, 90000, and 390000, Schmidt numbers of 2.53 and 700 and curvature ratios of 1.5, 2, and 2.5. The differences between the maximum axial velocity to average velocity (U_{max}/U_{ave}) predicted by the model and the experimental results reported in the literature was generally less than two percent. Simulation results showed that the ratio of the maximum Sherwood number obtained in the elbow to that obtained in fully developed pipe flow (Sh/Sh_p) decreased by Reynolds number (Re), Schmidt number (Sc) and curvature ratio (r/D). Maximum local mass transfer coefficient was observed at a distance of about one diameter downstream of the 90° elbow. Numerical predictions were in good agreement with experimental results reported in the literature.

KEY WORDS: Mass transfer; 90° bend; Turbulent flow.

INTRODUCTION

Mass transfer in fittings and bends is important in many industrial applications. As an instance, corrosion in bends is tightly related to mass transfer rate. Advances in Computational Fluid Dynamics (CFD) have provided solution for complex turbulent flows in complex geometries. For example CFD can be used to predict heat and mass transfer rates in duct geometries of practical relevance. In practical flow systems, the highest levels of mass transfer are often encountered in regions of disturbed flow associated with a change in flow structure induced by duct geometry. Changes in flow structure will also affect local turbulence level, making the variation in wall mass transfer rates even more difficult to predict. In such cases, a computational approach based on the use of a realistic turbulence model may be more helpful than correlations based on global flow parameters.

Due to the importance of the local mass transfer coefficients, several investigators conducted experiments for single-phase flows to determine the maximum mass transfer coefficients in 90° elbows and 180° bends.

Local mass transfer rates in circular pipe bends were measured experimentally [1]. It was reported that the maximum mass transfer rate was about 60% greater than that of the straight pipe with the same diameter. Local mass transfer coefficients in 45° and 180° bends with an $r/D=2.72$ were also measured [2]. Based on the measurements, it was concluded that Sh/Sh_p in 45° and 180° bends decreased by Reynolds number. Mass transfer in a two-dimensional 90° bend for a high Schmidt number fluid was numerically investigated using low Reynolds number $k-\varepsilon$ turbulence model [3]. Based on their

* To whom correspondence should be addressed.

+ E-mail: mmasr@cc.iut.ac.ir

1021-9986/15/4/113

9/\$/2.90

numerical simulations the mass transfer coefficient, k , was lower and higher along the inner and outer walls, respectively, than that of the straight duct. Mass transfer coefficients in elbows were predicted by using the low Reynolds number k - ε turbulence model [4]. By performing many CFD simulations a correlation to predict the maximum Sh/Sh_p in bends was developed [4]. It was shown that mass transfer rate is a function of Reynolds number, Schmidt number and curvature ratio (r/D). Sh/Sh_p were found to decrease slightly with Reynolds number, Schmidt number, and curvature ratio for moderate curvature ratios [5].

In this paper mass transfer rates in a three-dimensional 90° bend is investigated numerically. The RNG version of k - ε model was used for turbulence modeling. The effects of variation of Reynolds number (Re), Schmidt number (Sc) and curvature ratio (r/D) were studied.

THEORITICAL SECTION

Description of the computational models

Governing Equations of Fluid Motion

The continuity and momentum equations are given in equations (1) and (2), respectively:

$$\frac{\partial \rho}{\partial t} + \frac{\partial(\rho u)}{\partial x} + \frac{\partial(\rho v)}{\partial y} + \frac{\partial(\rho w)}{\partial z} = 0 \quad (1)$$

$$\left(\frac{\partial(\rho u)}{\partial t} + \frac{\partial(\rho u u_i)}{\partial x} + \frac{\partial(\rho v u_i)}{\partial y} + \frac{\partial(\rho w u_i)}{\partial z} \right) \Delta x \Delta y \Delta z = \Sigma F_i \quad (2)$$

where ΣF_i is the sum of the external forces on the control volume and is given by equation (3) in the x direction:

$$\Sigma F_x = \rho g_x - \frac{\partial p}{\partial x} + \mu \left(\frac{\partial^2 u}{\partial x^2} + \frac{\partial^2 u}{\partial y^2} + \frac{\partial^2 u}{\partial z^2} \right) \quad (3)$$

Where ρ is the fluid density, p and μ are the local pressure and viscosity of the fluid and u is the fluid velocity [6].

Component Continuity Equation:

The component continuity equation (conservation of component) is as follows:

$$\frac{\partial \rho_A}{\partial t} + \frac{\partial(\rho_A u)}{\partial x} + \frac{\partial(\rho_A v)}{\partial y} + \frac{\partial(\rho_A w)}{\partial z} = \quad (4)$$

$$D_{AB} \left(\frac{\partial^2 \rho_A}{\partial x^2} + \frac{\partial^2 \rho_A}{\partial y^2} + \frac{\partial^2 \rho_A}{\partial z^2} \right)$$

Where ρ_A is the concentration of diffusive component and D_{AB} is diffusion coefficient [6].

In many industrial applications flow in bends is turbulent and turbulent flow models are needed to calculate the flow field which is used in predicting mass transfer rates. The RNG version of k - ε turbulence model is claimed to be more appropriate for flows with curved stream lines [7] and was adopted in this work.

RNG k - ε model

The RNG model was developed using Renormalization Group (RNG) methods [8] to renormalize the Navier-Stokes equations, to account for the effects of smaller scales of motion. In the standard k - ε model the eddy viscosity is determined from a single turbulence length scale. In the RNG approach, results in a modified form of the epsilon equation attempting to account for the different scales of motion through changes to the production term can be used.

Transport equations

There are a number of ways to write the transport equations for k and ε , a simple interpretation where buoyancy is ignored is [8]:

$$\frac{\partial}{\partial t}(\rho k) + \frac{\partial}{\partial x_i}(\rho k u_i) = \quad (5)$$

$$\frac{\partial}{\partial x_j} \left[\left(\mu + \frac{\mu_t}{\sigma_k} \right) \frac{\partial k}{\partial x_j} \right] + P_k - \rho \varepsilon$$

$$\frac{\partial}{\partial t}(\rho \varepsilon) + \frac{\partial}{\partial x_i}(\rho \varepsilon u_i) = \quad (6)$$

$$\frac{\partial}{\partial x_j} \left[\left(\mu + \frac{\mu_t}{\sigma_\varepsilon} \right) \frac{\partial \varepsilon}{\partial x_j} \right] + C_{1\varepsilon} \frac{\varepsilon}{k} P_k - C_{2\varepsilon}^* \rho \frac{\varepsilon^2}{k}$$

Where the turbulent viscosity was calculated in the same manner as with the standard k - ε model as follow:

$$\mu_t = \rho C_\mu \frac{K^2}{\varepsilon} \quad (7)$$

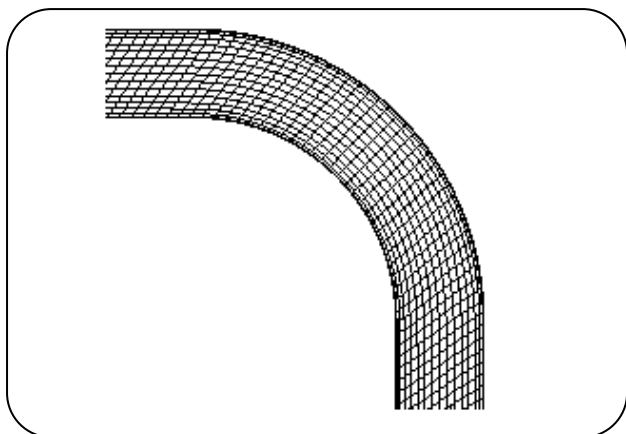


Fig. 1: Schematic scheme of grid points in the stream wise direction.

and

$$S = (2S_{ij}S_{ij})^{1/2} \quad (8)$$

and

$$P_k = \mu_t S^2 \quad (9)$$

and

$$\eta = Sk / \varepsilon \quad (10)$$

And

$$C_{2\varepsilon}^* = C_{2\varepsilon} + \frac{C_\mu \eta^3 (1 - \eta/\eta_0)}{1 + \beta \eta^3} \quad (11)$$

Constants

It is interesting to note that the values of all constants (except β) are derived explicitly in the RNG procedure. They are given below [8] with the commonly used values in the standard k- ε equation model in brackets for comparison:

$$C_\mu = 0.0845 \quad (0.09)$$

$$\sigma_k = 0.7194 \quad (1.0)$$

$$\sigma_\varepsilon = 0.7194 \quad (1.30)$$

$$C_{1\varepsilon} = 1.42 \quad (1.44)$$

$$C_{2\varepsilon} = 1.68 \quad (1.92)$$

$$\eta_0 = 4.38$$

$$\beta = 0.012 \quad (\text{Derived from experiment})$$

Flow Model Verification in a 90° Elbow

Velocity field in a 0.048 m diameter circular elbow with curvature ratio of 2.8 was measured making use of Laser-Doppler anemometry [9]. The same velocity field

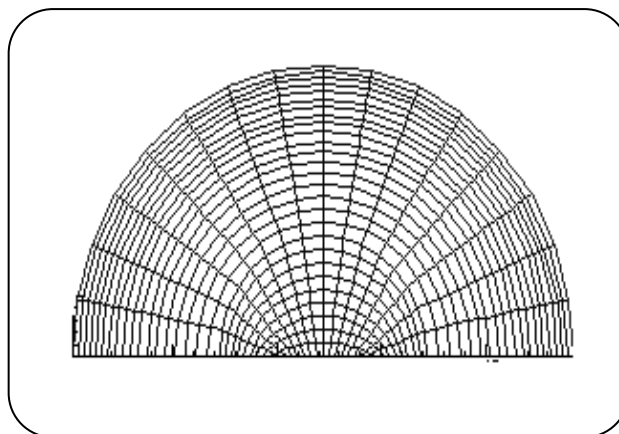


Fig. 2: Schematic scheme of grid points in the half of cross-section plan.

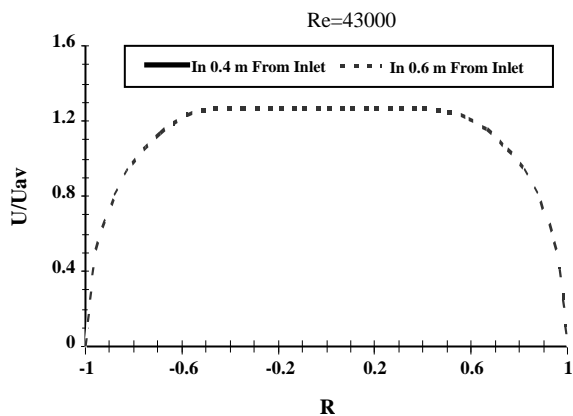
was simulated in this work and results were compared with measurements for model verification. The geometry consisted of 1 m long straight pipe, 0.048 m in diameter, followed by an elbow with curvature ratio of 2.8, followed by a straight pipe similar to the one used upstream of the elbow. The working fluid was water that entered the upstream straight pipe with a uniform velocity profile (0.92 m/s, Re=43000). Water velocity exited from the downstream straight pipe was assumed to be diffusion free for all flow variables. No slip velocity boundary condition was applied at walls. The total number of grid points used for solution was 162316 (146880 hexahedral structured cells) with 340 cells in the stream-wise direction as shown in Fig. 1. The total number of grid points in the half of the cross-section plane is 432 with 16 cells in the circumferential direction, 18 cells in the radial direction and 144 quadratic cells in the central part as shown in Fig. 2. A grid refinement study was performed by doubling the number of grid points in each direction. The differences between the maximum axial velocity to average velocity (U_{\max}/U_{ave}) was generally less than two percent. For example, the effect of increasing cells in the stream-wise direction on this parameter is shown in Table 1.

The predicted velocity profiles at two axial locations in the upstream straight pipe are shown in Fig. 3. It can be seen that at locations 0.4 and 0.6 m downstream of the pipe inlet the velocity profiles are exactly the same and therefore flow is fully developed.

The dimensionless velocity profiles at different axial locations in the bend are presented in Fig. 4. At the inlet of the bend, the maximum velocity is slightly close to the

Table 1: Comparison between (U_{max}/U_{av}) for different number of cells in the stream-wise direction ($Re=43000$).

Number of Cells	280	340	400	520
(U_{max}/U_{av})	1.4	1.38	1.38	1.39

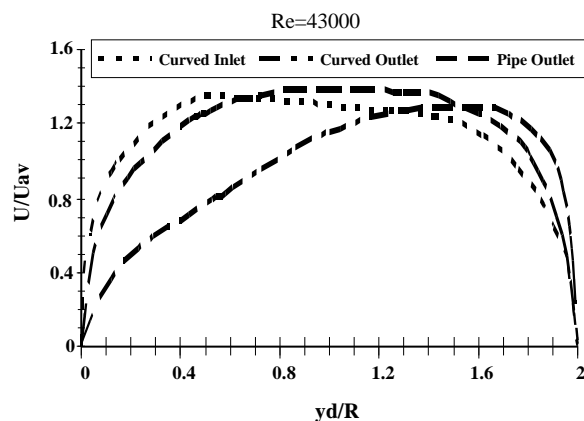
**Fig. 3: Velocity profiles at different axial locations at the symmetry plane.**

inner wall. At the bend outlet the maximum velocity has shifted towards the outer wall and the level of symmetry is much less than that observed at the entry of the bend. The asymmetry is due to the secondary flows developed in the bend. From the bend outlet secondary flows persist, but decrease gradually. At the downstream pipe outlet almost symmetric velocity profile was observed.

The predicted velocity profiles at $\theta = 75^\circ$ are compared with the measurements reported in [9] as shown in Fig. 5. It can be seen that simulation results agree relatively well with the measurements.

The flow model predictions downstream of the elbow were also carefully studied because the maximum mass transfer was reported to occur downstream of the exit of the elbows [4]. Fig. 6 shows the comparison of the predictions with the experimental data downstream of the elbow at $x/D=1$. Good agreement is observed between predicted and measured velocities downstream of the bend.

Since the maximum mass transfer occurs in the downstream pipe (about one to one half diameter-downstream of the elbow exit), where the predicted velocity profiles agree with the measurements, it was concluded that present flow model is good enough for prediction of mass transfer coefficients downstream of the elbow.

**Fig. 4: Velocity profiles at bend inlet, outlet and downstream pipe outlet.**

Mass transfer model verification

Mass transfer coefficients for sublimation of naphthalene in air were measured [10]. Naphthalene was casted as an elbow with curvature ratio of 1.5. Two air velocities were used in the experiments corresponding to Reynolds numbers of 9×10^4 , 3.9×10^5 . Schmidt number for binary gas mixture of naphthalene - air is 2.53. The same geometry was adopted in the present study to numerically predict mass transfer coefficients.

The total number of grid points used was 389918 (362340 hexahedral cells) with 330 cells in the stream-wise direction (similar to Fig. 1). The total number of grid points in the half of the cross-section is 1098 with 16 cells in the circumferential direction, 40 cells in the radial direction and 378 quadratic cells in the central part (similar to Fig. 2). Grid independency was studied as described previously. Using twice as much grid points as described, incremental effects were observed on velocity profiles and maximum Sherwood numbers. For mass transfer predictions, it was assumed that naphthalene concentration was zero at the upstream pipe inlet and the velocity profile was uniform. At the pipe wall, the dimensionless concentration of naphthalene C^* was one ($C^* = (C - C_{in}) / (C_w - C_{in})$), in this relation C_{in} is naphthalene concentration at the inlet of pipe and

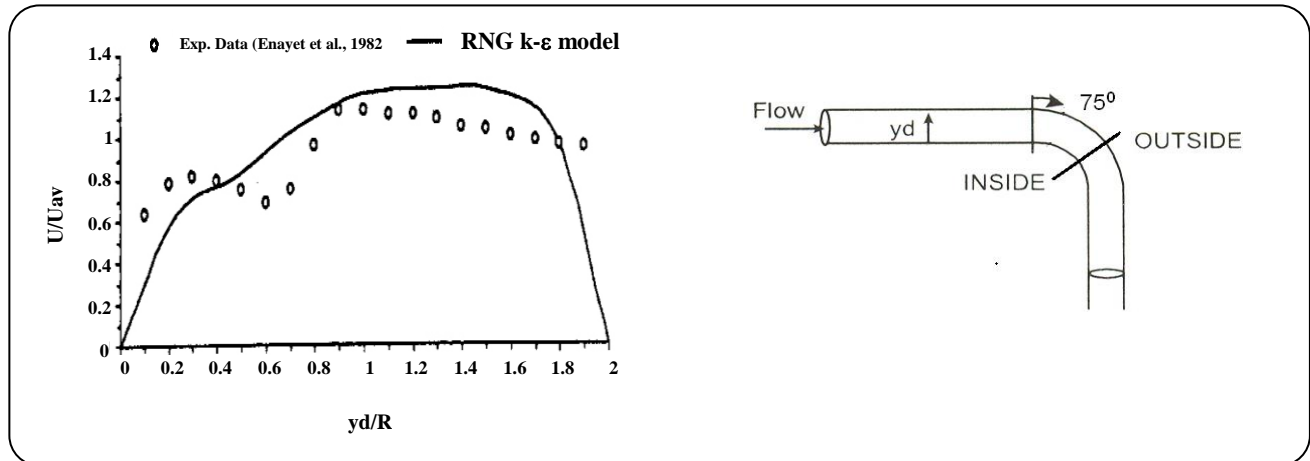


Fig. 5: Predicted velocity profile and experimental measurements from [9] at the 75° station.

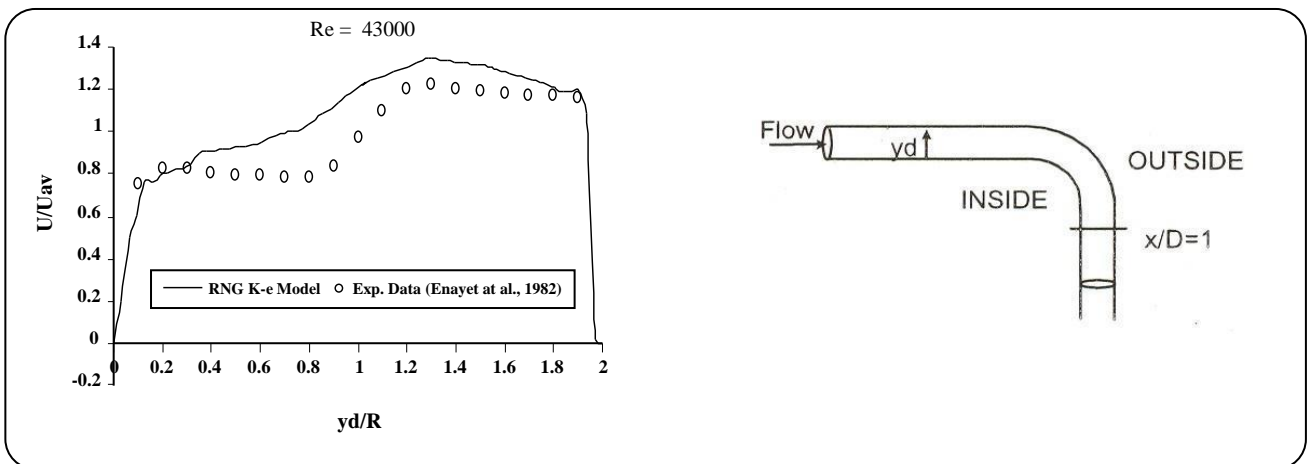


Fig. 6: Predicted velocity profiles and experimental data at $x/D=1$.

C_w is the concentration of naphthalene in the pipe wall) and no-slip velocity boundary condition was applied. The predicted results of the ratio of the local Sherwood number in the elbow to that of the fully developed flow in a pipe (Sh/Sh_p) are shown in Figs. 7 and 8. In these figures Sh_p has been calculated from equation (12) [11]:

$$Sh_p = 0.023Re^{0.8} Sc^{1/3} \quad (12)$$

For $Re=90000$ (Fig. 7), it is seen that Sh/Sh_p decreases from the downstream pipe inlet to about $\theta=10^\circ$ in the elbow. The ratio increases afterwards and max Sh/Sh_p was measured at $x/D=1$, which was 38% more than that of fully developed flow in a straight pipe with the same diameter. Also, from Fig. 8, it can be seen that the minimum mass transfer rate for $Re=390000$ occurs before the bend inlet and the max Sh/Sh_p is observed at the bend

outlet and calculated maximum Sherwood number is 32% more than that of fully developed flow in the straight pipe. This behavior may be resulted from development of strong pressured-driven secondary flows in the form of a pair of counter-rotating vortices in the stream-wise direction. Experimental measurements are also plotted in Figs. 7 and 8 showing the predictions agree with the experimental measurements.

RESULTS AND DISCUSSION

Concentration contours in a 90° elbow

Concentration contours at different axial locations are presented in Fig. 9. Inner (outer) surface of bend is on the left (right) of the figure. Upstream of the bend, concentration profiles are symmetric. As the flow progresses through the bend and from inlet to 30° station, no considerable change in concentration contours are observed.

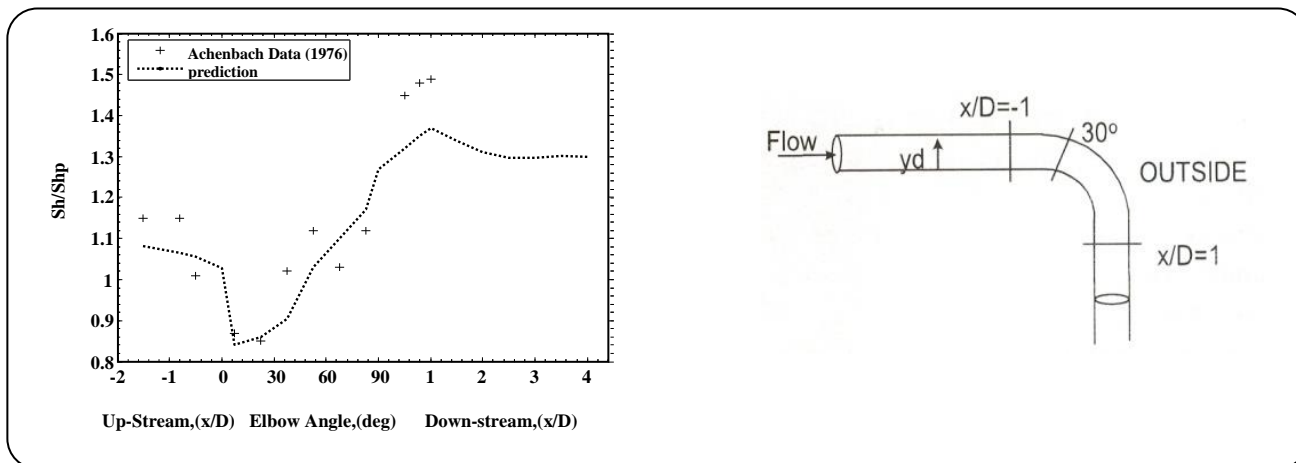


Fig. 7: Predicted mass transfer coefficients in a 90° elbow ($Re=9 \times 10^4$, $Sc=2.53$).

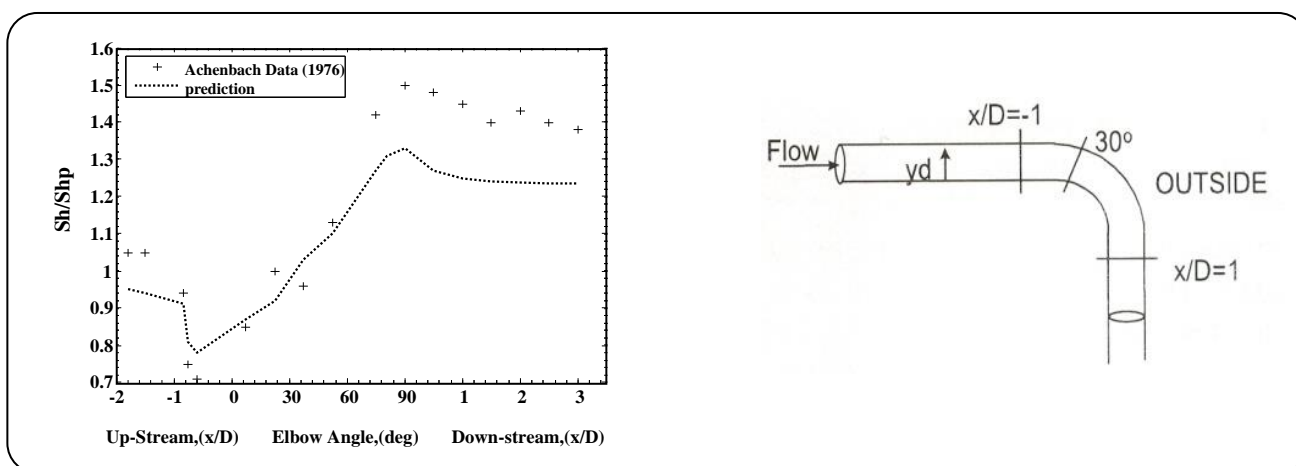


Fig. 8: Predicted mass transfer coefficients in a 90° elbow ($Re=3.9 \times 10^5$, $Sc=2.53$).

From $\theta = 30^\circ$ to the bend outlet the minimum concentration moves towards the outer wall. From the bend outlet to $x=10D$ the contours tend to become symmetric.

Mass Transfer Coefficients in Elbows

Mass transfer coefficient in elbow varies with the flow Reynolds number (Re), Schmidt number (Sc) and the curvature ratio (r/D). By performing CFD simulations based on different Reynolds numbers, Schmidt numbers and curvature ratios, the ratio of the local Sherwood number to that of fully developed flow (Sh/Sh_p) was obtained, in which Sh_p was calculated from Eq. (10). The simulation results for mass transfer as a function of the Reynolds number in a 90° elbow with $r/D=1.5$ and $Sc=2.53$ are shown in Fig. 10. It can be seen that Sh/Sh_p decreases by increasing Reynolds number. The same trend was previously reported [2].

The effect of curvature ratio (r/D) was studied on Sh/Sh_p at $Re=13500$ and $Sc=2.53$. The results are shown in Fig. 11. It can be seen that Sh/Sh_p decreases by the curvature ratio. The same trend was previously reported [12]. Predicted Sh/Sh_p for $r/D=1.5$ with $Re=9 \times 10^4$, as a function of the Schmidt number is shown in Fig. 12. It can be observed that Sh/Sh_p is greater for gases than that of liquids.

Wang and Shirazi have developed a correlation for the max Sh/Sh_p in elbows by performing many CFD simulations using the low Reynolds number k- ϵ turbulence model [4]. They reported that their results were in good agreement with the experimental data of Achenbach [10]. Their correlation is shown in equation (13):

$$\max(Sh / Sh_p) = 0.68 + (1.2 - 0.044 \ln(Re)) e^{-0.065r/D} + \frac{0.58}{\ln(Sc + 2.5)} \quad (13)$$

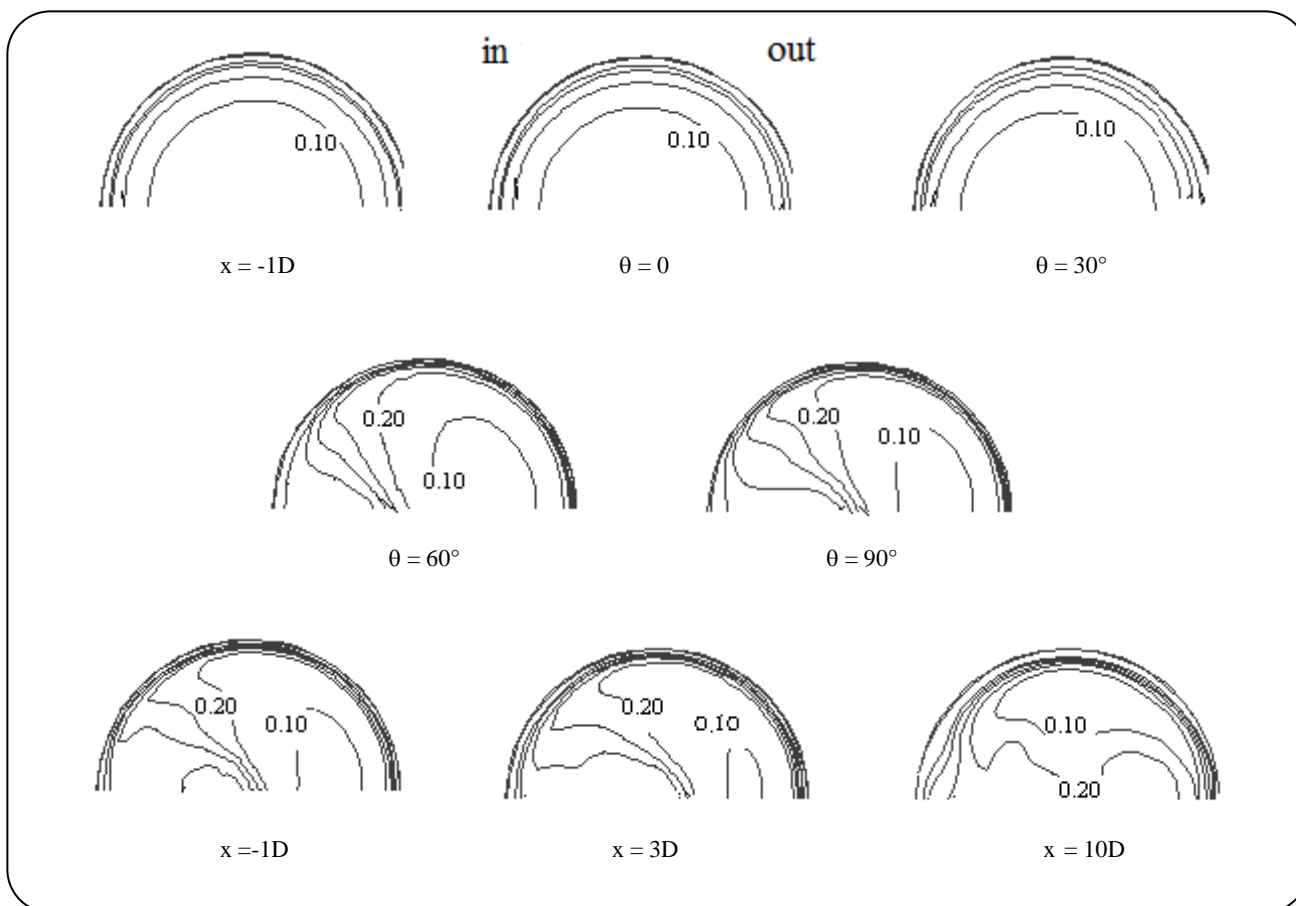


Fig. 9: Contours of dimensionless concentration at different axial locations of the 90° bend ($Re=13500$, $r/D=1.5$, $Sc=2.53$).

This relation shows that the max Sh/Sh_p decreases as the Reynolds number (Re), Schmidt number (Sc) and curvature ratio (r/D) increases. The comparison between predictions of the present study and equation (13) for different Reynolds and Schmidt numbers are given in Tables 2 and 3.

Although there are some differences in absolute values of obtained Sh/Sh_p from numerical simulations and equation 13, the percentage increase by decreasing Re or Sc agrees excellently. Coney has experimentally investigated the mass transfer in bends and developed an equation for Sh/Sh_p [12]:

$$\frac{Sh}{Sh_p} = 1 + 2.2 \left(\frac{R}{r}\right)^{1.2} \left(\frac{L}{D}\right)^{0.75} \quad (14)$$

D is the inside pipe diameter, R the radius of the pipe ($R=D/2$), r the mean radius of the elbow, and L is the length along the axis of the curved section of the elbow. For a 90° elbow, $L=\pi r/2$, and Eq. (14) becomes:

$$\frac{Sh}{Sh_p} = 1 + 1.343 \left(\frac{r}{D}\right)^{-0.45} \quad (15)$$

Eq. (15) shows that Sh/Sh_p is a sole function of the curvature ratio. This correlation suggests that the Reynolds number does not have an influence on the Sh/Sh_p . The comparison between predictions by numerical simulations and Eqs. (13) and (15) for max Sh/Sh_p is given in table 4. From table 4, it is seen that the max Sh/Sh_p decreases as the ratio of r/D increases. Although there are some differences in values of the numerical predictions and Eqs. (13) and (15), the percentage changes in Sh/Sh_p are in good agreement.

CONCLUSIONS

Three-dimensional computational flow simulations were performed and mass transfer predictions were developed in a 90° elbow. Generally, upstream of the bend inlet the concentration profile is almost symmetric. As the flow progresses through the bend distinguishably

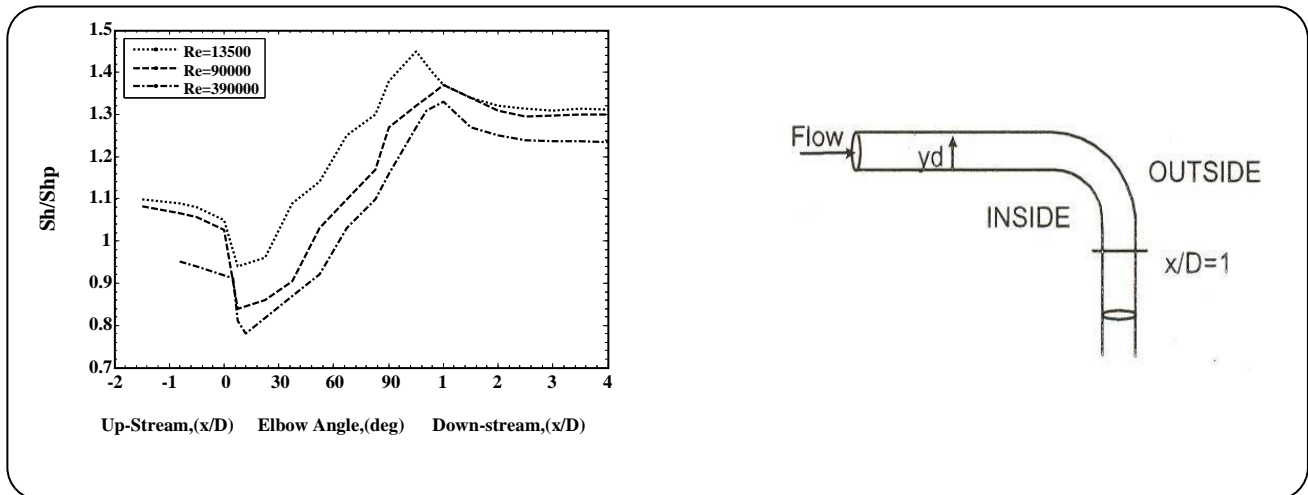


Fig. 10: Variation of (Sh/Sh_p) with the Reynolds number ($Sc = 2.53, r/D = 1.5$).

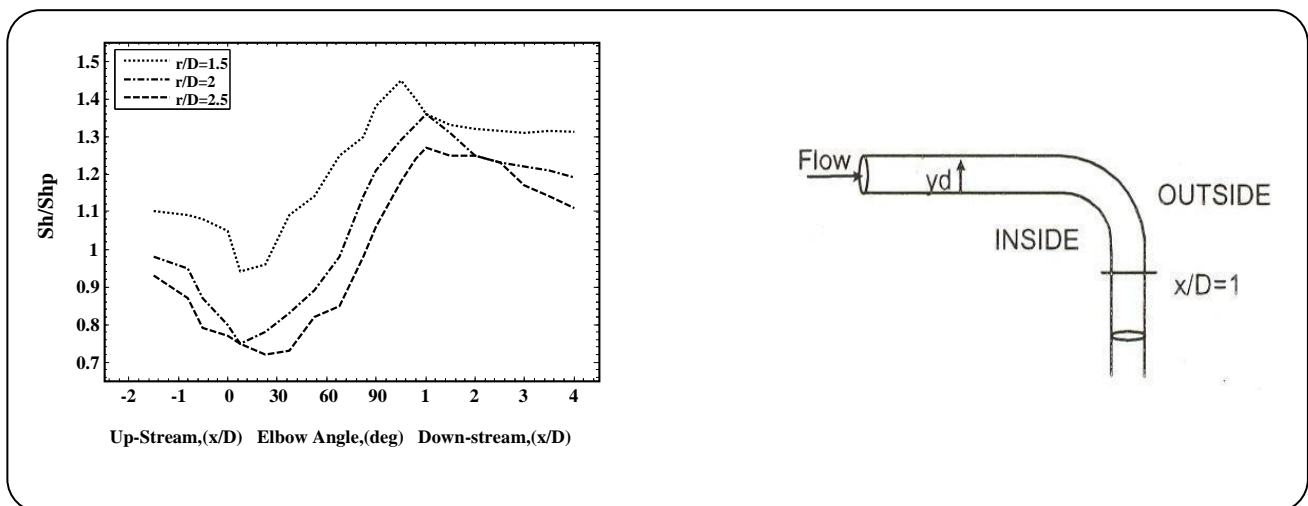


Fig. 11: Variation of (Sh/Sh_p) with r/D ($Re = 13500, Sc = 2.53$).

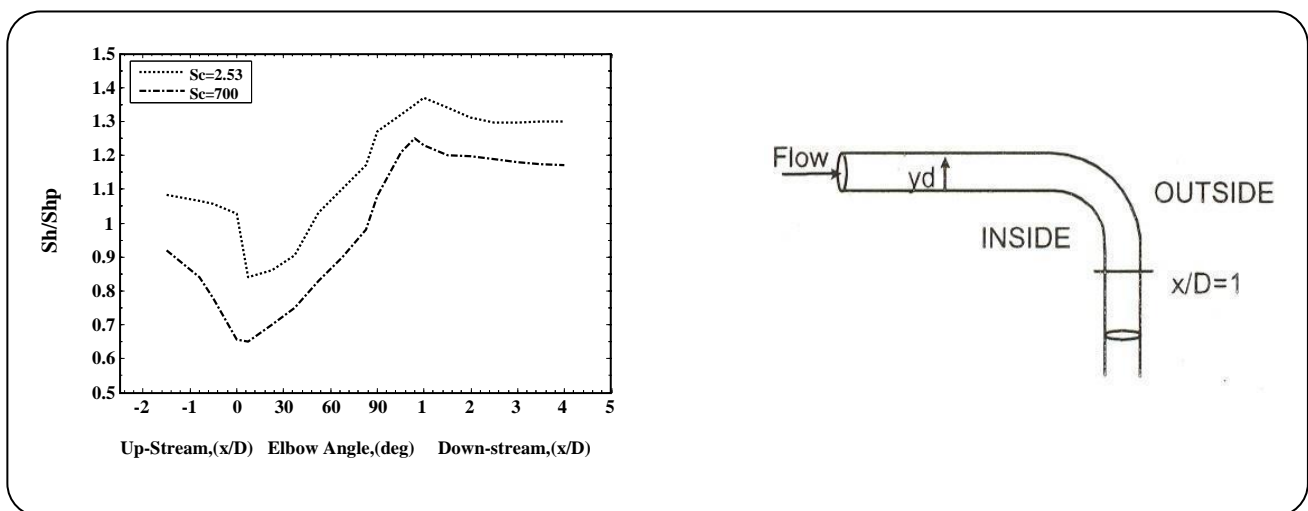


Fig. 12: Variation of (Sh/Sh_p) with the Schmit number ($Re = 9 \cdot 10^4, r/D = 1.5$).

from $\theta = 30^\circ$, the minimum concentration gets close to the outer wall. Maximum (Sh/Sh_p) predictions are in good agreement with measurements. Maximum mass transfer rate was observed between the bend outlet and a distance one diameter downstream of the elbow exit for different Re , r/D and Sc investigated in this work. Sh/Sh_p were found to decrease slightly with the flow Reynolds number, Schmidt number, and r/D for moderate r/D values. The maximum Sh/Sh_p was calculated to be 1.46 for $Re=13500$, $Sc=2.53$ and $r/D=1.5$.

Nomenclature

C	Concentration, kmol/m ³
D	Inside pipe diameter, m
D _{AB}	Diffusion coefficient, m ² /s
F	External body forces on the control volume, N
g	Acceleration of gravity, m/s ²
i, j	Direction of axial coordinate
k	Turbulent kinetic energy, m ² /s ²
L	Length along the axis of the curved section of the elbow, m
P	Local pressure, Pa
P _k	Production rate of turbulent kinetic energy
r	Radius of the curvature of the elbow, m
R	Pipe radius, m
Re	Reynolds number
S	Modulus of the mean rate of strain tensor
Sc	Schmidt number
Sh	Sherwood number
Sh _p	Sherwood number for fully developed pipe flow
t	Time
u, v, w	Fluid velocity components, m/s
yd	Distance from inner wall of the bend, m

Greek symbols

ε	Turbulent dissipation rate
η	
μ	Fluid viscosity, kg/m.s
μ_t	Turbulent viscosity, kg/m.s
ρ	Fluid density, kg/m ³

Received : Aug. 11, 2013 ; Accepted : Jan. 22, 2015

REFERENCES

- [1] Sprague P.J., "Mass Transfer and Erosion Corrosion in Pipe Bends", *Ph.D. Thesis*, University of Exeter, England, (1984).
- [2] Sprague P.J., Patrick M.A., Wragg A.A., Coney M.W.E., Mass Transfer and Erosion Corrosion in Pipe Bend, in: "Proceedings of the Eighth Congress of European Federation of Corrosion", 18.1-18.6 (1989).
- [3] Bergstrom D.J.B., Adamopoulos T., Postlethwaite J., Numerical Prediction of Wall Mass Transfer Rates in Turbulent Flow Through a 90° Two-Dimensional Bend, *The Canadian Journal of Chemical Engineering.*, **76**: 728-737 (1998).
- [4] Wang J., Shirazi S.A., A CFD Based Correlation for Mass Transfer Coefficient in Elbows, *Int. J. Heat and Mass transfer*, **44**: 1817-1822 (2001).
- [5] Asadi T., Nasr Esfahany M., Numerical Prediction of Mass Transfer Coefficient in Turbulent Flow Through a 90° Bend, "Proceedings of CHT-08 ICHMT International Symposium on Advances in Computational Heat Transfer , (ICHMT)", Marrakech, Morocco, *CHT-08-137* (2008)
- [6] Bird R.B., Stewart W.E., Lightfoot E.N.t, "Transport Phenomena", John Wiley & Sons, New York (2001).
- [7] Yin M., Shi F., Xu Z., Renormalization Group Based $\kappa - \varepsilon$ Turbulence Model for Flows in a Duct with Strong Curvature, *International Journal of Engineering Science*, **34**: 243-248 (1996).
- [8] Yakhot V., Orszag S.A., Thangam S., Gatski T.B., Speziale C.G., Development of Turbulence Models for Shear Flows by A Double Expansion Technique, *Physics of Fluids*, **4**: 1510-1520 (1992).
- [9] Enayet M., Gibson M., Yianneskis M., Laser Doppler Measurements for Laminar and Turbulent Flow in Pipe Bend, *Int. J. Heat Fluid Flow*, **3**: 213-220 (1982).
- [10] Achenbach E., Mass Transfer from Bend of Circular Cross-Section to Air, in: "Future Energy Production Systems", Academic Press, New York., **1**: 327-337 (1976).
- [11] Treybal R.E., "Mass Transfer Operation", McGraw Hill, New York, (1980).
- [12] Coney M.W.E., "Erosion Corrosion: The Calculation of Mass Transfer Coefficients", *CEGB Report RD/L/N197/80 CERL*, (1980).